coatings

MDPI

Article

PDINN as an Efficient and Environmentally Friendly Corrosion Inhibitor for Mild Steel in HCl: A Comprehensive Investigation

Jiakai Kuang [1], Shaopeng Fu [2], Jiaqi Song [3], Lanlan Ma [3], Xueqi Liu [3], Zezhou Liang [4], Jianfeng Li [3,*] and Jinpeng Dai [1,*]

[1] School of Civil Engineering, Lanzhou Jiaotong University, Lanzhou 730070, China; 15777110731@163.com
[2] School of Mechanical Engineering, Lanzhou Jiaotong University, Lanzhou 730050, China; fsp2545667562@163.com
[3] School of Materials Science and Engineering, Lanzhou Jiaotong University, Lanzhou 730070, China; 13919093973@163.com (J.S.); 17389593449@163.com (L.M.); 18854357602@163.com (X.L.)
[4] School of Electronics Science & Engineering, Faculty of Electronic and Information Engineering, Xi'an Jiaotong University, Xi'an 710049, China; zezhouliang@hotmail.com
* Correspondence: ljfpyc@163.com (J.L.); daijp@seu.edu.cn (J.D.)

Abstract: The screening of environmentally friendly, efficient and high-temperature-resistant organic corrosion inhibitors represents a significant means of reducing metal losses in industrial production. In this study, we investigated using aliphatic amine-functionalized perylene-diimide (PDINN) to inhibit Q235 steel in 1 M HCl media. The results show that PDINN significantly inhibits corrosion of Q235 steel in 1 M HCl. It is of greater significance that PDINN's inhibition is unresponsive to temperature fluctuations in the corrosive environment, maintaining an efficiency of 86.5% at an ambient temperature of 328 K. DFT and MD analyses indicate that the exceptional inhibitory capacity of PDINN is closely associated with the extensive conjugated structure within the molecule, where it is firmly adsorbed on the Fe (110) via π-electrons.

Keywords: Q235 steel; PDINN; corrosion inhibition; HCl; electrochemical



Academic Editor: Peter Rodič

Received: 19 February 2025
Revised: 11 March 2025
Accepted: 17 March 2025
Published: 19 March 2025

Citation: Kuang, J.; Fu, S.; Song, J.; Ma, L.; Liu, X.; Liang, Z.; Li, J.; Dai, J. PDINN as an Efficient and Environmentally Friendly Corrosion Inhibitor for Mild Steel in HCl: A Comprehensive Investigation. *Coatings* **2025**, *15*, 352. https://doi.org/10.3390/coatings15030352

Copyright: © 2025 by the authors. Licensee MDPI, Basel, Switzerland. This article is an open access article distributed under the terms and conditions of the Creative Commons Attribution (CC BY) license (https://creativecommons.org/licenses/by/4.0/).

1. Introduction

Corrosion is a major problem in industrial production, and it can cause significant damage to metal objects over time. Due to its high tensile strength, ductility and low cost, mild steel is widely used in industries including bridges and buildings, oil pipelines and chemical plants [1–4]. The extraction of oil and gas often involves corrosive media, including carbon dioxide, hydrogen sulfide and chloride ions. These corrosive substances can cause significant corrosion of carbon steel, particularly at low pH and high chloride ion concentrations [5,6]. Many cost-effective methods have been developed to prevent acid damage to steel, including the use of corrosion-resistant metals (e.g., stainless steel, aluminum), the use of coating materials (e.g., paint), sacrificial anodes to protect the cathode and the use of corrosion inhibitors [7,8]. All of these methods can inhibit damage to steel, and corrosion inhibitors have been identified as a widely used and effective method [9].

Corrosion inhibitors can be classified into two main categories: inorganic and organic (OCIs) [10,11]. Generally, OCIs adsorb onto the steel surface to form a protective shield, which can occur through chemisorption or physisorption, relying on the inhibitor structure [12,13]. The inhibition process is dynamic and the corrosion inhibitor gradually replaces the corrosion particles (H_2O, Cl^-, etc.) on the metal surface [14]. OCIs are also known as adsorption corrosion inhibitors based on their ability to adsorb and modify

corrosion processes. The protective effect of OCIs on metals is closely related to their own chemical structure and dosage, the properties and surface charges of metal itself, corrosion intensity and environmental temperature [15,16]. Compared to inorganic products, OCIs have the advantages of low toxicity and environmental benefits. Therefore, their corrosion-inhibiting properties in acidic media on carbon steel have been extensively investigated.

It has been found that inhibitor performance is closely related to their electronic properties [17,18]. Compounds that contain five/six-membered rings and heteroatoms including N, O and S in their structure are ideal inhibitors [19]. As these heteroatoms can form chemical bonds with iron, they protect the steel from corrosion. It is clear from our literature review that various organic substances are already being used for corrosive inhibition of metals in various corrosive media [20,21]. Polyimide derivatives serve as corrosion inhibitors due to their abovementioned characteristics and greater electron donor/acceptor capacity. A.K. Kushwaha et al. [17] investigated the interaction between pyromellitic diimide (PMDI) and zinc oxide at the atomic scale to elucidate its potential as an inhibitor. The PMDI compound was functionalized with methyl/diamine groups in order to enhance its corrosion inhibition and strengthen its interaction with galvanized steel. The results showed that F-PMDI functionalized with diamine groups (inh3) exhibited the best corrosion inhibition performance and had a strong interaction with zinc oxide. Wang et al. [22] synthesized a novel bridged perylene diimide self-assembled molecule (PDI-E) via imidazole solvothermal methods. Through a combined experimental and computational approach, the authors demonstrated that PDI-E could form a dense, ordered film on aluminum alloy substrates via π-π stacking and terminal bridging interactions. Electrochemical impedance spectroscopy revealed an impressive film resistance of 38,525 $\Omega \cdot cm^2$ and a corrosion current density reduction to 2.837×10^{-7} A/cm^2, significantly outperforming the bare substrate. This work underscores the critical role of PDI's aromatic core and functionalized side chains in achieving horizontal molecular alignment and steric shielding against corrosive agents. A comparative study [23] of perylene bis-imide derivatives (e.g., $C_{38}H_{18}N_2O_{10}$, $C_{34}H_{32}N_4O_4$) demonstrated that nitrogen-rich side chains enhanced electron donation to steel surfaces, forming hydrophobic monolayers via covalent Fe−N bonding and π-electron interactions. Cyclic corrosion tests revealed that these compounds reduced blistering by 80% under NaCl mist exposure, with corrosion inhibition efficiencies exceeding 92% at a 0.5% pigment volume concentration (PVC). These findings emphasize the role of multifunctional adsorption sites (e.g., amines, hydroxyls) in stabilizing metal–coating interfaces.

This work focuses on the corrosion inhibitory properties of amino N-oxide functionalized perylene-diimide (PDINN) as an acidic medium for steel. The inhibition properties of this organic compound were evaluated by electrochemical tests and micromorphological analysis, and the inhibition mechanism was enhanced using quantum chemical calculations (QCs) and molecular dynamics (MD).

2. Materials and Methods

2.1. Material and Solution

PDINN was synthesized in our lab, and the procedures followed were from a previously reported study (Figure 1) [24].

A solution of 1 M hydrochloric acid was prepared by diluting 37% hydrochloric acid with ultra-pure water to simulate an aggressive environment. The working electrode is mild steel (Q235 steel) and its chemical composition is shown in Table S1. As shown in Figure S1, a copper conductor was soldered to the end face of a rectangular body with machined dimensions of 10 mm × 10 mm × 5 mm, with the reverse side as the working surface and the other surfaces sealed with epoxy resin. Prior to all tests, the surfaces to be tested

were abraded with emery paper (120#–2000#). Subsequently, they were degreased with acetone, rinsed thoroughly with water, dried and prepared for use. Furthermore, various concentrations of PDINN solutions were prepared by introducing specific quantities of PDINN powder into a pre-established 1 M HCl solution.

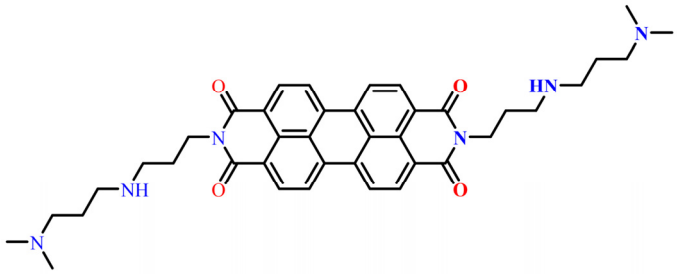


Figure 1. Chemical structure of PDINN.

2.2. Electrochemical Tests

The electrochemical experiments involved in this study were conducted with the CHI660E. Experiments were conducted using a three-electrode system: the working electrode was made of mild steel (Figure S1, working area = 1 cm^2) and Pt was employed as a counter electrode, while a saturated calomel electrode served as the reference electrode. After immersing the prepared electrodes in an acid solution for 30 min and establishing a stable open-circuit potential (OCP), electrochemical impedance spectroscopy (EIS) tests were performed at frequencies from 100 kHz to 0.01 Hz and amplitudes of 5 mV. In addition, potentiodynamic polarization (PDP) tests were performed from ±300 mV relative to the OCP with a scan rate of 1 mV s^{-1} [9].

2.3. Surface Characterization

The surface of the metal was examined after corrosion using SEM-EDS. The surface was polished and immersed in a PDINN solution containing the optimal concentration (300 ppm) and in a solution without PDINN for 12 h at 298 K, then removed, cleaned and dried. The sample surface was observed using a Gemini 500 field emission scanning electron microscope (ZEISS, Jena, Germany) equipped with an Oxford UltimMax 65 EDS.

2.4. Quantum Chemical Calculations

An optimized conformation of PDINN at the level of B3LYP (D3)/6-31 g * was obtained using Gaussian16 [25]. At the same time, SMD was used to consider the polarization of H_2O [26]. In addition, the distribution of front molecular orbitals (highest occupied orbital, HOMO; lowest unoccupied orbital, LUMO) and their energy gap ($\Delta E = E_{LUMO} - E_{HOMO}$) and other quantum chemical parameters were also obtained. Finally, the electrostatic potential (ESP) of optimized PDINN was analyzed and the data were post-processed using Multiwfn [27] and VMD [28] software.

2.5. MD Simulations

Fe (110) is the densest and most stable of the common crystalline surfaces of iron [29]. An optimized Fe single cell was cut using the Visualizer function in Materials Studio to create the Fe (110) surface, which was then expanded to produce a surface with dimensions of 27.3 Å × 27.3 Å × 14.2 Å. Amorphous cell modules were used to build amorphous structures containing 400 H_2O molecules, one inhibitor molecule, five chloride ions and five hydrogen ions which were then attached to the metal surface using a 30 Å vacuum layer [30].

The Smart algorithm was used to optimize the above structure in at least 2000 steps, after which it simulated the structure using the Forcite module. In the course of the calculation, 5 layers of Fe atoms underneath the adsorbed structure were frozen, whereas other atoms were relaxed by the strain. The simulation was conducted using the NVT ensemble with a time step of 1 fs, a total time of 500 ps and a simulated temperature of 298 K. The entire simulation was performed using the COMPASSII force field. The non-bonded interactions were assigned to an atom-based summation where the electrostatic interactions were summed using the Ewald summation. The cut-off radius was 12.50 Å [30]. The energy of adsorption ($E_{adsorption}$) after the simulation is calculated using Equation (1) [31]:

$$E_{\text{adsorption}} = E_{\text{total}} - (E_{\text{surface + solution}} + E_{\text{solution + Inhibitir}}) + E_{\text{solution}} \quad (1)$$

where E_{total} represents the overall energy, $E_{surface+solution}$ is the energy of combining the iron and the H_2O layer, and $E_{solution+Inhibitor}$ means the total energy of H_2O and then inhibitor.

3. Results and Discussions

3.1. OCP Test

The OCP plot (Figure 2) revealed that an immersion time of 1800 s was sufficient to obtain a stable OCP for both inhibited and uninhibited systems. Unprotected steel exhibits the most negative potential, probably due to the metal forming an oxide film in air that dissolves rapidly in solution. In addition, the OCP gradually shifts in a positive direction with increasing PDINN concentration, suggesting that it has a much greater effect on metal dissolution compared to the cathodic behavior of the corrosion process [28,29].

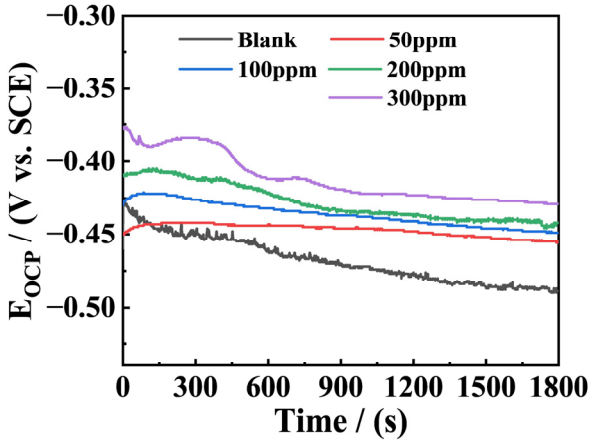


Figure 2. The OCP of Q235 steel at different PDINN levels in 1 M HCl medium.

3.2. EIS Measurement

EIS curves for steel electrodes were obtained for various concentrations of PDINN at 298 K. Based on the Nyquist plot (Figure 3a), it can be observed that each capacitive loop is an imperfect semicircle, and their diameters increase with the concentration of PDINN. Imperfect capacitive loops are the product of frequency dispersion due to the rough electrode surface and the unevenness of the active sites caused by corrosion [9,32]. Thus, it can be shown that PDINN adsorbs on abrasive surfaces. The impedance curves generated at different corrosion inhibitor concentrations (including blank) are almost identical in shape, indicating that the incorporation of PDINN has not altered the corrosion response. In the Bode plot (Figure 3b), all curves have only one time constant; their highest phase angle and impedance modulus indicate that the corrosion reaction is completed in one step, and both increase with increasing PDINN levels, implying that the unevenness of the electrode surface decreases with PDINN coverage.

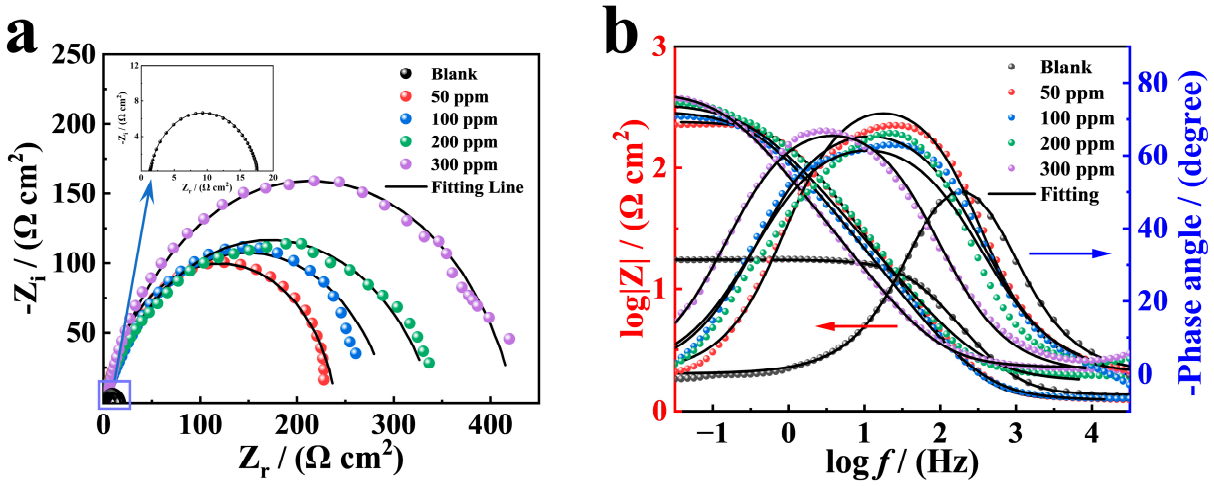


Figure 3. Nyquist (**a**) and Bode plots (**b**) of Q235 steel in a blank solution and in solutions containing different levels of PDINN.

The results of fitting the EIS using the most satisfactory equivalent circuit diagram (Figure 4) are given in Table 1. Here, the charge transfer resistor (R_{ct}) and the solution transfer resistor (R_s) are connected in series and in parallel with the double-layer constant phase element (CPE). Since the steel/electrolyte interface is a non-ideal capacitor, the CPE is used instead of a capacitive element to elucidate the behavior of the bilayer. Its impedance, Z_{CPE}, is calculated by Equation (2) [33,34]:

$$Z_{CPE} = (Y_0)^{-1}(j\omega)^{-n} \quad (2)$$

where Y_0 denotes the scale factor, ω is the angular frequency, j expresses the imaginary root (j = $(-i)^{1/2}$) and n is the phase shift ($-1 \leq n \leq 1$). It illustrates the degree of surface roughness or inhomogeneity of the electrode. In conjunction with this, the double-layer capacitance (C_{dl}) is obtained from Equation (3) [35]:

$$C_{dl} = Y_0 (2\pi f_{max})^{n-1} \quad (3)$$

where f_{max} is the frequency corresponding to the maximum imaginary part of the impedance. Table 1 reveals the salient increase in R_{ct} after the addition of PDINN. The corrosion inhibition performance is usually generated by this parameter using Equation (4) [36]:

$$IE_{EIS} = \frac{R_{ct} - R_{ct,0}}{R_{ct}} \times 100\% \quad (4)$$

Table 1. EIS parameters of the electrodes with PDINN at various concentrations in 1 M HCl.

Inhibitor	Conc. (ppm)	R_s (Ω cm^2)	R_{ct} (Ω cm^2)	Y_0 ($\times 10^{-5}$ s^n Ω^{-1} cm^{-2})	n	C_{dl} ($\times 10^{-5}$ F cm^{-2})	IE_{EIS}%
Blank	0	1.35	16.23	44.60	0.88	43.62	—
PDINN	50	1.23	239.20	35.76	0.88	29.55	93.21
	100	1.23	294.70	34.35	0.80	28.85	94.49
	200	1.77	326.90	31.58	0.79	27.25	95.04
	300	1.87	423.50	25.71	0.82	26.09	96.17

As is evident, the excellent inhibition of PDINN at low concentrations, as well as the marginal improvement in inhibition efficiency (ΔIE% $\approx$ 3%–4%) despite a sixfold increase in PDINN concentration (50–300 ppm), suggests saturation of adsorption sites at lower concentrations.

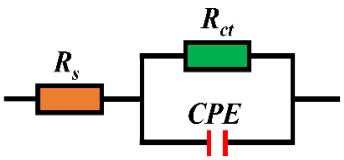


Figure 4. Equivalent circuits for fitting EIS.

The Helmholtz model (Equation (5)) [37,38] can be used to explain the bilayer capacitance, where d and S represent the film thickness and electrode area, respectively, ε^0 represents the air dielectric constant and ε represents the local dielectric coefficient.

$$C_{dl} = \frac{\varepsilon^0 \varepsilon S}{d} \quad (5)$$

Figure 5 illustrates the relationship between different C_{dl} values and the active area (S) in the presence of PDINN. It is clear that the relationship is linear (R^2 = 0.888) and that ε and d are constant. This indicates that the adsorption membrane is a monolayer and of constant thickness [39]. With increasing concentrations of PDINN, C_{dl} decreases as more molecules are adsorbed onto surface, as can also be seen in Table 1, which means that PDINN replaces the water molecules at the interface and increases the thickness of the adsorption film, thus protecting the metal substrate from corrosion. Also, the barrier reduces the area of electrodes that may be oxidized [40,41].

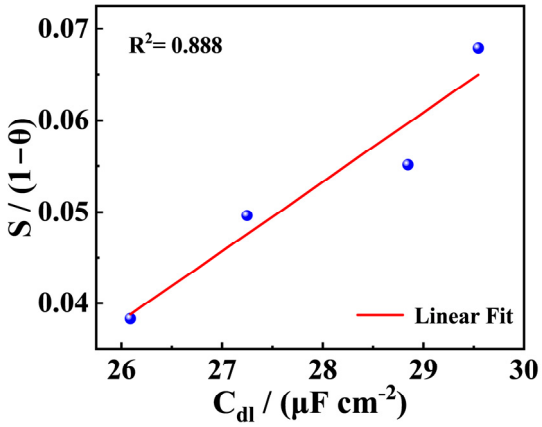


Figure 5. Relationship between electrode active area S and bilayer capacitance C_{dl}.

3.3. PDP Measurements

Figure 6 shows the kinetic potential polarization curves of Q235 steel at 298 K with various levels of PDINN. The relevant corrosion kinetic parameters are presented in Table 2, where E_{corr} refers to corrosion potential, and β_a and β_c are the anodic and cathodic slopes, respectively. IE_{TP} can be acquired from Equation (6) [42]:

$$IE_{TP} = \frac{I_{corr,\,0} - I_{corr}}{I_{corr,\,0}} \times 100\% \quad (6)$$

where $I_{corr,0}$ and I_{corr} are corrosion current densities without and with PDINN in the electrolyte. The anodic and cathodic branches shifted to lower values of PDINN relative to HCl medium, and this phenomenon became more pronounced the higher the concentration of the inhibitor. Furthermore, the change in E_{corr} is below ±85 mV for different concentrations of PDINN compared to the blank solution, indicating that PDINN inhibited both metal dissolution and reduction reactions [43]. Furthermore, Table 2 shows that the potential differences of Q235 steel in different concentrations of inhibition solution and blank solu-

tion are 0.035, 0.053, 0.059, and 0.061. This monotonically increasing potential difference suggests that PDINN may primarily affect the metal dissolution at the anode directly rather than indirectly reducing the corrosion rate through the inhibition of the cathodic reaction of the corrosion process, as reported for other cathodic corrosion inhibitors in the literature.

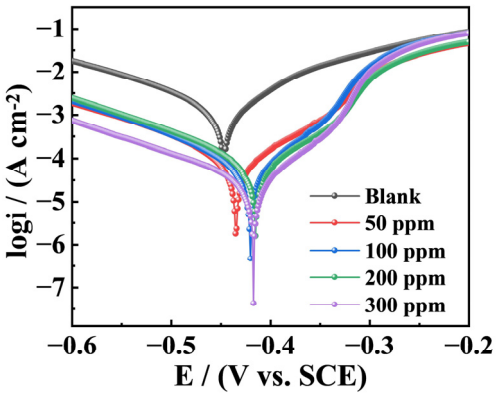


Figure 6. PDP curves for Q235 steel in blank solution and in solutions with different concentrations of PDINN.

Table 2. PDP curve fitting parameters for steel corrosion with different concentrations of PDINN.

Inhibitor	Conc. (ppm)	E_{corr} (V)	βa (mv/Dec)	−βc (mv/Dec)	I_{corr} (μA/cm^2)	IE_{TP} (%)
Blank	0	−0.446	115.26	157.01	1134.02	—
PDINN	50	−0.411	56.84	123.70	65.46	94.23
	100	−0.393	36.19	233.34	38.06	96.64
	200	−0.387	35.36	77.38	20.12	98.23
	300	−0.385	31.32	132.55	17.53	98.45

3.4. Thermodynamic Parameters and Adsorption Isotherm

The adsorption process of PDINN was analyzed based on the EIS results. The surface coverage (θ) of various doses of PDINN is comparable to the inhibitor efficiency (θ = IE_{EIS}). The isotherm models of Langmuir were fitted to our data using the results from the aforementioned electrochemical experiments, as shown in Figure 7.

$$\frac{C_{\text{inh}}}{\theta} = \frac{1}{K_{\text{ads}}} + C_{\text{inh}} \tag{7}$$

where C_{inh} represents the concentration of PDINN, while K_{ads} is the adsorption–desorption equilibrium constant. Figure 5 illustrates that the thickness of the adsorbed film on the mild steel surface remains constant at 298 K. This suggests that the adsorbed organic molecules form a monolayer of essentially constant thickness on the metal, as predicted by the Langmuir model (Figure 7). Additionally, the lack of interaction between PDINN indicates that it appears as a homogeneous, cohesive layer on the Q235 steel surface.

After determining an appropriate adsorption model, we were able to calculate the K_{ads}. Using this value, one can calculate the free energy of standard adsorption (ΔG^0_{ads}). The relationship between them is given by Equation (8) [44]:

$$\Delta G^0_{ads} = -RTln\left(1 \times 10^6 K_{ads}\right) \tag{8}$$

This relationship allows us to understand the thermodynamic driving forces behind the adsorption action and to evaluate the protection layer's stability on the surface. Based on the literature [45,46], the −20/40 kJ/mol criterion is typically employed to ascertain

whether inhibitor molecules are physically or chemically adsorbed on metal surfaces. In this work, −32.17 kJ/mol falls between the typical ranges for physical and chemical adsorption, suggesting that the inhibitor may act through both mechanisms on the active surface of the metal.

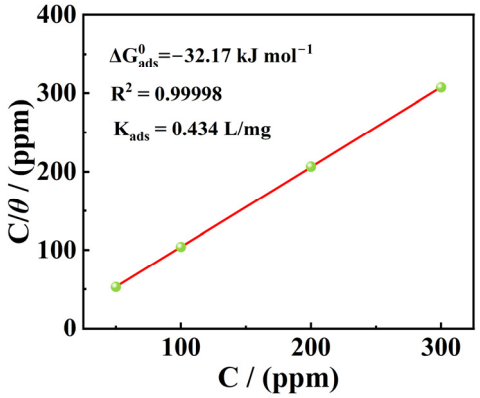


Figure 7. Fitting results for sorption isotherm at 298 K of Langmuir model.

3.5. Influence of Temperature

The impact of temperature on the IE% of PDINN was evaluated through PDP tests on mild steel at varying temperatures in both blank and inhibition solutions. The outcomes are presented in Figures 8 and 9, with the corresponding parameters displayed in Table S2. The results demonstrate that the inhibition effect of PDINN exhibits a gradual response to temperature fluctuations. At 328 K, the efficiency of the inhibition process was found to be 86.5%. These findings suggest that the PDINN inhibitor is effective at protecting the metal from corrosion over a range of temperatures. Subsequently, the temperature dependence of I_{corr} can be modeled via the Arrhenius equation [47]:

$$\ln(i_{\text{corr}}) = \ln(K) - \frac{E_a}{RT} \tag{9}$$

Here, K is the pre-exponential factor. E_a is the activation energy, R is the gas constant (8.314 J/mol·K) and T is the temperature. E_a was obtained from Figure 10, and the results are presented in Table 3. Upon adding the PDINN, the energy barrier of the corrosion process became higher, indicating that it makes it more difficult to achieve the electrochemical corrosion of Q235 steel. Other thermodynamic parameters, such as the activation enthalpy (ΔH_a) and activation entropy (ΔS_a), are crucial for understanding the energy barrier and disorder changes during the corrosion process. These parameters are governed by the transition state theory equation [48]:

$$i_{\text{corr}} = \frac{RT}{Nh} \exp\left(-\frac{\Delta H_a}{RT}\right) \exp\left(\frac{\Delta S_a}{R}\right) \tag{10}$$

where N is Avogadro's number, h is Planck's constant and T is temperature. The enthalpy (ΔH_a) rises from 33.7 kJ/mol (uninhibited) to 67.09 kJ/mol (with PDINN), driven by endothermic π metal bonding outweighing water desorption. Concurrently, entropy (ΔS_a) shifts from −91.1 to 6.82 kJ/mol, highlighting disordered water layer disruption as the dominant entropic contribution over molecular adsorptive losses.

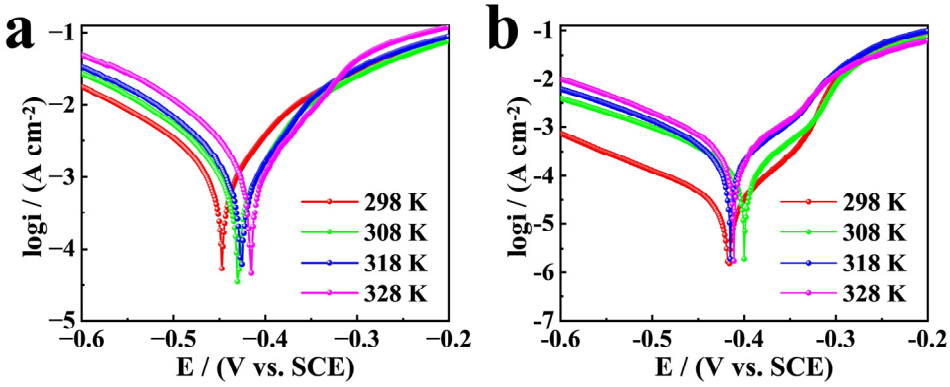


Figure 8. The influence of temperature on the corrosive procedure of the electrode (**a**) without and (**b**) containing 300 ppm PDINN.

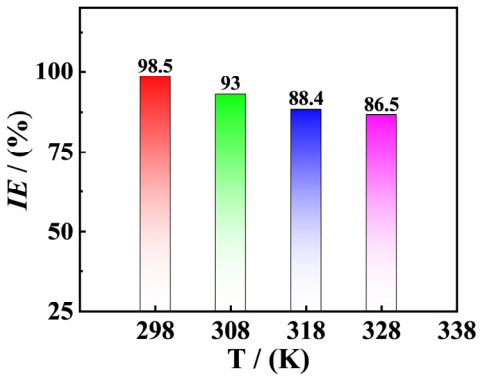


Figure 9. Inhibition efficiency of 300 ppm PDINN on electrode in HCl medium at various temperatures.

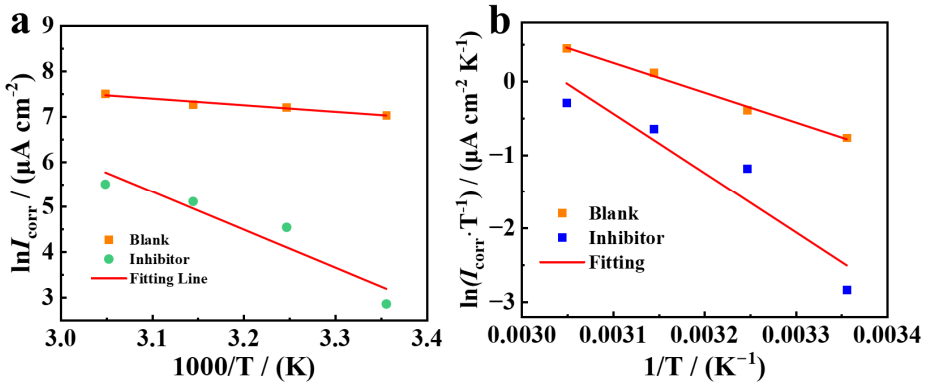


Figure 10. Arrhenius curves (**a**) and transition state diagrams (**b**) of Q235 steel in absence and presence of 300 ppm PDINN.

Table 3. *Ea* for Q235 steel in blank solution and with addition of 300 ppm PDINN.

Inhibitor	E_a/(kJ·mol^{-1})	K/(μA cm^{-2})	R^2	ΔH_a/(kJ·mol^{-1})	ΔS_a/(kJ·mol^{-1})
Blank	12.06	0.15×10^6	0.927	33.7	−91.1
PDINN	69.69	40×10^{12}	0.855	67.09	6.82

3.6. Surface Morphological Studies

Figure 11a presents the surface morphology of polished Q235 carbon steel. After immersion in HCl solution without PDINN for 12 h, the surface of Q235 steel was severely corroded and numerous corrosion pits and products were generated (Figure 11b). Upon

addition of the prepared inhibitor, the steel surface became smooth with minimal corrosion products, indicating that the adsorption film provided good protection for the metal (Figure 11c). The findings of the EDS analysis are consistent with this perspective. Furthermore, elemental analysis of the corroded Q235 steel surface revealed a discernible reduction in Fe content and the emergence of N (Figure S2). The Fe originates from the steel substrate, whereas the N is attributed to the PDINN corrosion inhibitor. This elemental shift conclusively corroborates the formation of a PDINN-derived adsorption film on the metal surface.

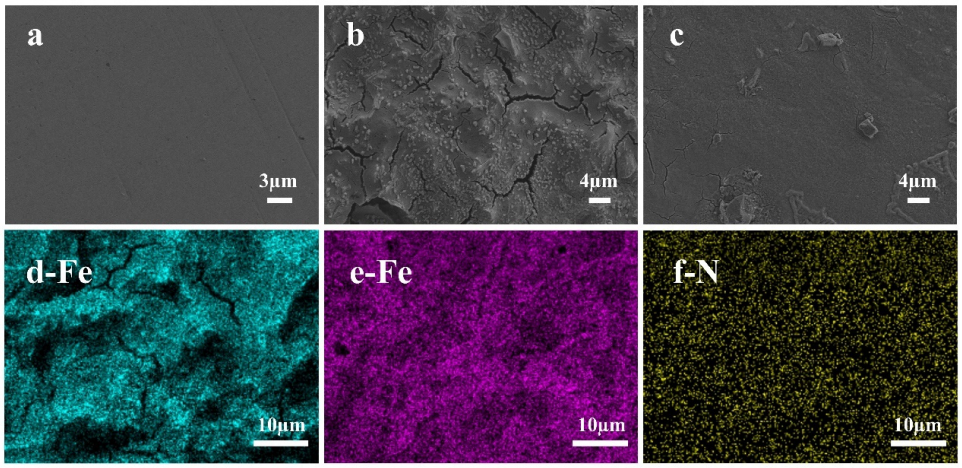


Figure 11. Corrosion morphology of steel surfaces: (**a**) not immersed; (**b**) immersed in HCl-0 ppm; (**c**) immersed in HCl-300 ppm. Elemental distribution of steel surfaces: (**d**) immersed in HCl-0 ppm; (**e**,**f**) immersed in HCl-300 ppm.

3.7. Computational Studies

Figure 12a–c illustrate the optimized geometry and HOMO-LUMO distribution of the PDINN molecule. The reactivity of the inhibitor is determined by the HOMO and LUMO, which indicate its affinity to donate or accept electrons. The investigation revealed that the HOMOs of PDINN were predominantly distributed on the N atoms at the terminal end of the extended chain, while the LUMOs were chiefly concentrated on the central ring and proximate oxygen atoms. To further understand the potential interaction between PDINN and mild steel, the electrostatic potential (ESP) of PDINN was analyzed. The ESP is a measure of the distribution of charge within a molecule and can be used to predict sites of attack for electrophiles and nucleophiles. The ESP isosurface of PDINN, shown in Figure 12d, illustrates the distribution of positive (blue) and negative (read) electrostatic potential within the molecule. The minimum value of ESP (V_{min}) enables the spatial location of the unpaired electrons and the active site of compounds when adsorbed on the electrode surface to be determined. The results reveal that the regions around the N-H and C=O atoms have negative values, while the central ring region are positive. The distribution of van der Waals (vdW) coloring ESP of PDINN was calculated (Figure 12e). The vdW surface is a representation of the molecular surface and can provide insight into the distribution of charge within a molecule in relation to its surface. The results show that the electrostatic potential is more negative on the O of the N-H and C=O groups (−144.89 kJ/mol, −134.22 kJ/mol) and more positive on the C located in the central ring region. This reaffirms the above view that mild steel may act electrophilically by bonding to the ESP-negative region of the inhibitor molecule, while the ESP-positive C atom may function in the nucleophilic reactivity of PDINN.

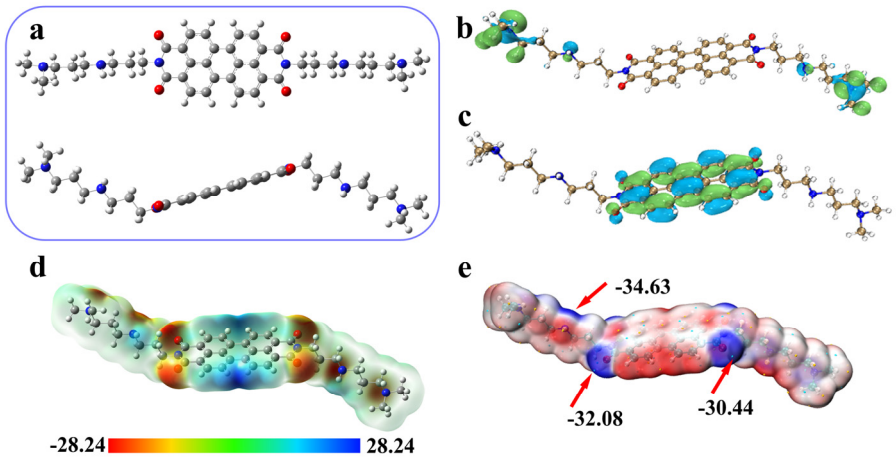


Figure 12. Optimized structure (**a**), HOMO (**b**), LUMO (**c**), ESP isosurface (**d**) and ESP mapped vdW surface (**e**).

Mulliken Atomic Charge (MAC) provides insight into finding adsorption sites for inhibitors. In particular, the atoms with the largest negative charge in the molecule and the Fe (110) surface tend to interact most strongly. Figure S2 illustrates the PDINN MAC. It can be seen that the O atoms and part of the C atoms in the central ring carry the largest number of negative charges, suggesting that the atoms have the highest electron density and are strongly bonded to the surface.

In general, the interactions between PDINN and electrodes depend on its E_{HOMO} and E_{LUMO} as well as the Fermi level of iron (−5.177 eV) [49]. A higher E_{HOMO} and a lower E_{LUMO} indicate greater electron donation and electron acceptance, respectively [50]. As shown in Figure 13, the E_{LUMO} of PDINN (−3.684 eV) is above −5.177 eV, whereas the E_{HOMO} of PDINN (−5.831 eV) is below the Fermi level. This suggests that electrons can leap from the HOMO of PDINN to the metal surface. Furthermore, the energy needed to excite an electron from a molecule, represented by ΔE, is often an important factor in describing the reactivity of static molecules. A low value of ΔE (2.1475 eV) in this study indicates high inhibition efficacy.

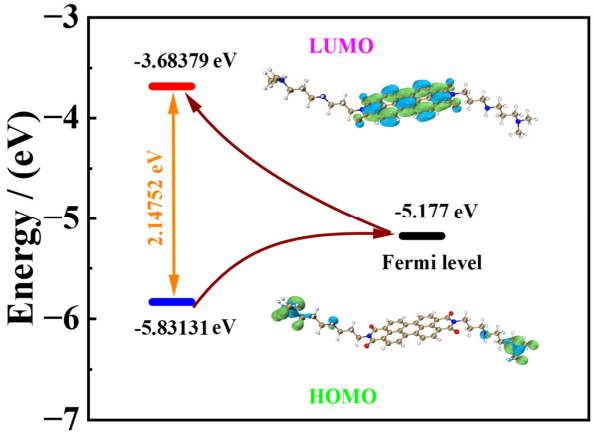


Figure 13. The calculated values for the relevant parameters including E_{HOMO}, E_{LUMO} and ΔE for PDINN.

To identify the local reactive sites in the inhibitor molecules, various quantum chemical descriptors were calculated, including the Fukui indices (f_k^+, f_k^-), global hardness ($\eta = -\frac{1}{2}(E_{LUMO} - E_{HOMO})$), global softness ($s = -\frac{1}{\eta}$), electronegativity ($\chi = -\frac{1}{2}(E_{LUMO} + E_{HOMO})$), electrophilicity ($\omega = \frac{\chi^2}{2\eta}$), local softness ($s_k^{\pm} = s f_k^{\pm}$), local

electrophilicity ($\omega_k^{\pm} = \omega\, f_k^{\pm}$) and dual local descriptors ($f_k^2 = f_k^+ - f_k^-, \Delta s_k = s_k^+ - s_k^-$, $\Delta\omega_k = \omega_k^+ - \omega_k^-$). In general, higher f_k^+ or f_k^- values of atoms exhibit a greater ability to receive or donate electrons, respectively, and are therefore more susceptible to attack by nucleophilic or electrophilic agents [20]. For PDINN (Figure 14), numerous carbon atoms and O22, O25, O36 and O37 have high f_k^+ values, indicating a strong susceptibility to nucleophilic attack at these positions. On the other hand, the side-chain atoms including N32 and N44 have high f_k^- values, and these atoms are vulnerable to electrophilic attack. In addition, Figure 14 shows the local dual descriptors ($f_k^2, \Delta s_k, \Delta\omega_k$) for PDINN. In general, site descriptors that tend toward pro-nuclear attack have negative values, while positive values indicate that these sites tend toward electrophilic attack [51,52]. The $f_k^2, \Delta s_k, \Delta\omega_k$ values of the PDINN side-chain atoms are less than zero, while those of the central ring are greater than zero, indicating that the atoms of the central ring may accept electrons from the Fe surface and adsorb onto the surface.

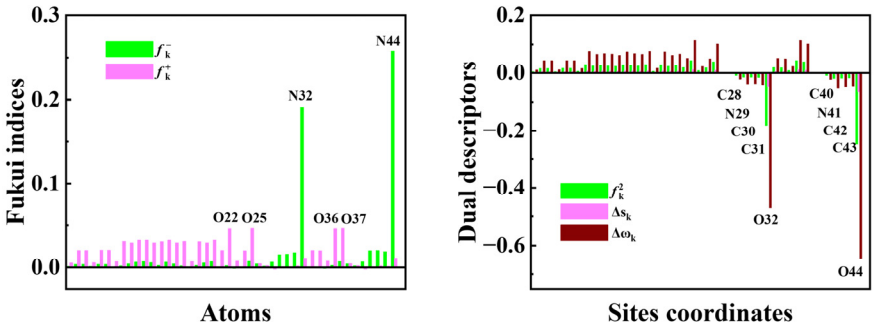


Figure 14. Fukui indices and dual descriptors of PDINN.

3.8. Molecular Dynamic Simulations

The adsorption forms of corrosive species and inhibitors on surfaces were investigated by molecular dynamics simulations (MD). The lower the adsorption energy, the stronger the inhibitor–metal interaction. Their adsorption configurations on the surface are illustrated in Figure 15, and the adsorption energies on the surface have been obtained (Table 4). The adsorption energies of all species are negative, indicating that they can spontaneously interact with Fe (110) surfaces. The order of adsorption energies is $H_2O > Cl^- > H_3O^+ >$ PDINN, a trend that suggests that PDINN can effectively displace corrosive particles and provide a surface protection film [30].

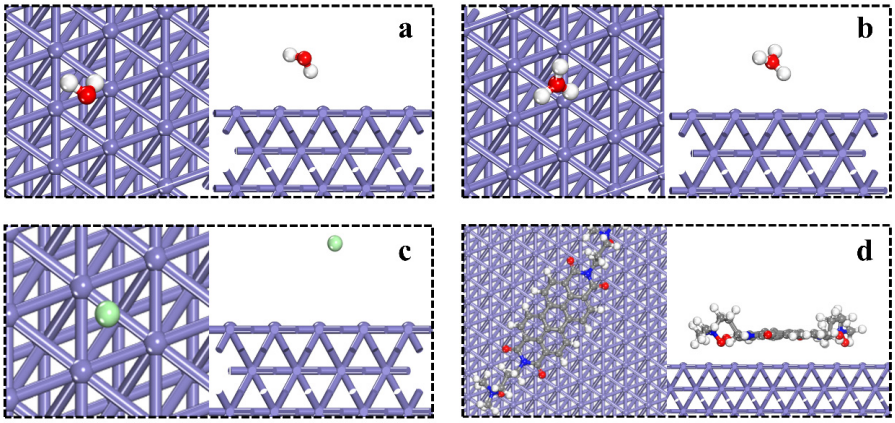


Figure 15. Final adsorption configuration for (**a**) H_2O, (**b**) H_3O^+, (**c**) Cl^- and (**d**) PDINN on Fe (110) surface.

Table 4. Free energy of adsorption (E_{ads}) of various corrosive particles on iron surfaces.

Particles	E_{ads} (kJ/mol)
H_2O	−6.505
H_3O^+	−7.251
Cl^-	−6.920
PDINN	−301.710

In order to examine the diffusion rate of corrosive particles (H_2O, H_3O^+, Cl^-) in blank H_2O and in the presence of adsorbed inhibitor films, we tracked the motion of these particles using mean square displacement (MSD) analysis. The mean square displacement (MSD) was then used to calculate the diffusion coefficient (D) for the corrosive particles [53,54]:

$$MSD(\mathrm{t}) = \frac{1}{\mathrm{N}_\alpha}\sum_{\mathrm{i}=1}^{\mathrm{N}_\alpha}\langle|\mathrm{r_i}(t) - \mathrm{r_i}(0)|^2\rangle \tag{11}$$

$$D = \frac{1}{6}\lim_{t\to\infty}\frac{dMSD(t)}{dt} \tag{12}$$

Figure 16 shows the diffusion model for corrosive particles in H_2O and inhibitor films (PDINN), as well as the corresponding diffusion coefficients (D) listed in Table 5. The MSD curves for the various corrosives in the water box and in the adsorbed PDINN films are shown in Figure S5. Figure S5 shows the temperature and energy of the system over time during the simulation. As can be seen in Table 6, the values of the diffusion coefficient for corrosion particles in PDINN film are significantly lower than in the blank H_2O phase. This result suggests that the inhibitor films adsorbed on Q235 steel can impede the diffusion process of corrosion particles effectively, thus preventing the corrosion process of mild steel.

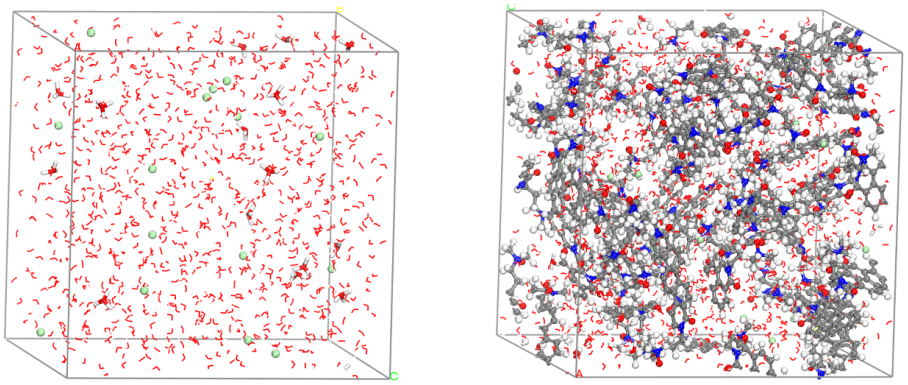


Figure 16. Diffusion model for H_2O, H_3O^+ and Cl^- (expressed as CPK) in H_2O phase and adsorbed inhibitor films (PDINN).

Table 5. D (m^2/s) of H_2O, H_3O^+ and Cl^- in H_2O box and PDINN films.

Diffusion Models	H_3O^+	H_2O	Cl^-
H_2O box	2.03×10^{-9}	3.45×10^{-9}	2.03×10^{-9}
PDINN box	4.40×10^{-10}	1.31×10^{-9}	6.96×10^{-10}

Table 6. The E_{ads} of PDINN on a liquid phase/Fe (110) surface containing corroded particles.

E_{Total} (kJ/mol)	$E_{Surface+Solution}$ (kJ/mol)	$E_{Solution+Inhibitir}$ (kJ/mol)	$E_{Solution}$ (kJ/mol)	$E_{Adsorption}$ (kJ/mol)
1.308×10^6	1.301×10^6	0.118×10^6	0.111×10^6	−247.7

Figure 17 shows a side (a) and top (b) view of the adsorption pattern of PDINN on the Fe (110) in a solution containing corroded particles, as determined by molecular dynamics simulations. The central ring of PDINN is adsorbed onto the Q235 steel surface in a horizontal position, and coupled with the results of the QCs, this may be the result of the O atoms near the central ring providing electrons to the surface and some of the C atoms receiving electrons from the surface. Table 6 shows the adsorption energies of the PDINN monomer adsorbed on Fe (110) surfaces in aqueous solutions containing corrosive particles at 298 K. The results are negative, indicating that PDINN can spontaneously adsorb on Fe surfaces.

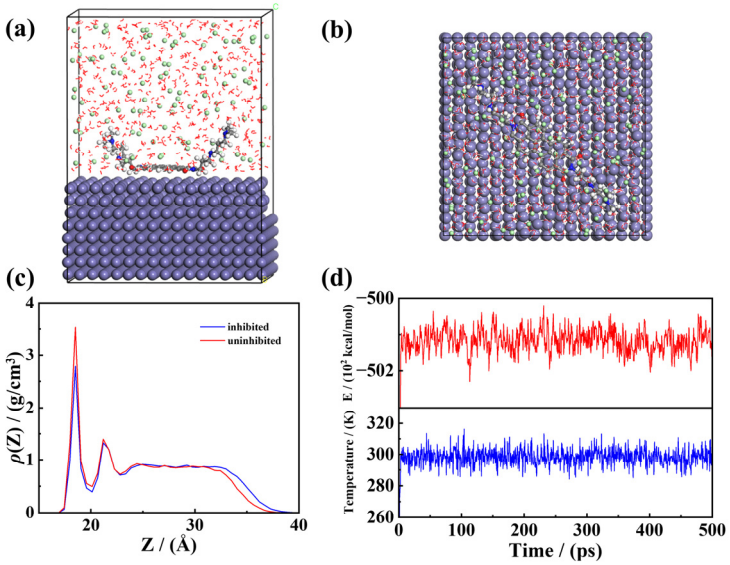


Figure 17. The final adsorption configuration of PDINN on a liquid phase/Fe (110) surface containing corroded particles: (**a**) side view and (**b**) top view. (**c**) The density distribution of H_2O along the z-axis at the interface and (**d**) the variations in temperature (blue) and energy (red) during the simulation.

Figure 17c illustrates the relative concentration distribution of H_2O along the Z-direction on Fe (110); the results show that the addition of inhibitors results in more H_2O being removed from the steel surface. This indicates that the protective film formed as a result of the adsorption of PDINN prevents H_2O from approaching the metal surface, thus protecting the metal from corrosion. The stability of the molecular dynamics simulation was confirmed by monitoring the total energy and temperature of the system over time (Figure 17d). Both parameters equilibrated within 500 ps, demonstrating that the simulation achieved thermodynamic balance, thereby validating the trajectory analysis for inhibitor adsorption behavior.

4. Conclusions

In this work, PDINN was demonstrated as an effective corrosion inhibitor for mitigating the degradation of Q235 steel in 1 M HCl. The electrochemical results indicate that this molecule can effectively inhibit the corrosion of Q235 steel in 1 M HCl. The inhibition ability of PDINN increases with increasing concentration, and it exhibits a satisfactory inhibition efficiency (98.45%) at 300 ppm. Most importantly, the fluctuation in the inhibition ability of PDINN with temperature was minimal, and the excellent performance (86.5%) was maintained at higher temperatures. The adsorption behavior of the compound in question follows the Langmuir isothermal adsorption model for monomolecular layer adsorption. It may act as a corrosion inhibitor by directly inhibiting the dissolution of the metal anode.

From the molecular structure, it can be seen that PDINN adsorbs in a conjugated structure and parallel to Fe (110). The C and O atoms in the conjugated structure are possible adsorption sites, and the π-electrons in the molecule may interact with the 3d orbitals of Fe. However, it is more often the case that the molecule accepts electrons from the Fe surface. Finally, the work presented in this thesis provides a foundation for the screening and development of novel organic materials as corrosion inhibitors for mild steel in HCl.

Supplementary Materials: The following supporting information can be downloaded at: https://www.mdpi.com/article/10.3390/coatings15030352/s1, Table S1. Chemical composition of working electrode (Q235) (wt %). Table S2. Corrosion kinetic parameters for Q235 in 1 M HCl without and with 300ppm of PDINN at different temperatures. Figure S1. Working electrode. Figure S2. Elemental content of surface of Q235 steel without immersion (**a**) and after immersion in 1 M HCl hydrochloric acid containing 300 ppm PDINN (**b**). Figure S3. Optimized structure of inhibitor and its Mulliken atomic charges (MACs). Figure S4. The MSD curves for various corrosive species in the aqueous phase (H_2O box) and in the adsorbed PDINN membrane. Figure S5. The variation in temperature and energy during the MD simulation.

Author Contributions: Investigation, J.S., L.M. and X.L.; software, Z.L.; writing—original draft, J.K. and S.F.; writing—review and editing, J.D. and J.L. All authors have read and agreed to the published version of the manuscript.

Funding: This. work was supported by the National Natural Science Foundation of China (52368032), the Science and Technology Program of Gansu Province (24JRRA286), the Natural Science Foundation of Gansu Province (25JRRA228) and the Innovation and Entrepreneurship Training Program for College Students of Lanzhou Jiaotong University (DC2510732CX0868).

Institutional Review Board Statement: Not applicable.

Informed Consent Statement: Not applicable.

Data Availability Statement: The data are contained within the article.

Conflicts of Interest: The authors declare no conflicts of interest.

References

1. Sharma, S.; Ganjoo, R.; Saha, S.K.; Kang, N.; Thakur, A.; Assad, H.; Sharma, V.; Kumar, A. Experimental and Theoretical Analysis of Baclofen as a Potential Corrosion Inhibitor for Mild Steel Surface in HCl Medium. *J. Adhes. Sci. Technol.* **2022**, *36*, 2067–2092. [CrossRef]
2. Ganjoo, R.; Sharma, S.; Thakur, A.; Assad, H.; Kumar Sharma, P.; Dagdag, O.; Berisha, A.; Seydou, M.; Ebenso, E.E.; Kumar, A. Experimental and Theoretical Study of Sodium Cocoyl Glycinate as Corrosion Inhibitor for Mild Steel in Hydrochloric Acid Medium. *J. Mol. Liq.* **2022**, *364*, 119988. [CrossRef]
3. Bashir, S.; Lgaz, H.; Chung, I.-M.; Kumar, A. Effective Green Corrosion Inhibition of Aluminium Using Analgin in Acidic Medium: An Experimental and Theoretical Study. *Chem. Eng. Commun.* **2021**, *208*, 1121–1130. [CrossRef]
4. Khan, G.; Basirun, W.J.; Kazi, S.N.; Ahmed, P.; Magaji, L.; Ahmed, S.M.; Khan, G.M.; Rehman, M.A.; Badry, A.B.B.M. Electrochemical Investigation on the Corrosion Inhibition of Mild Steel by Quinazoline Schiff Base Compounds in Hydrochloric Acid Solution. *J. Colloid Interface Sci.* **2017**, *502*, 134–145. [CrossRef]
5. Tiu, B.D.B.; Advincula, R.C. Polymeric Corrosion Inhibitors for the Oil and Gas Industry: Design Principles and Mechanism. *React. Funct. Polym.* **2015**, *95*, 25–45. [CrossRef]
6. Ueda, M. 2006 FN Speller Award Lecture: Development of Corrosion-Resistance Alloys for the Oil and Gas Industry—Based on Spontaneous Passivity Mechanism. *Corrosion* **2006**, *62*, 856–867. [CrossRef]
7. Bashir, S.; Thakur, A.; Lgaz, H.; Chung, I.-M.; Kumar, A. Corrosion Inhibition Performance of Acarbose on Mild Steel Corrosion in Acidic Medium: An Experimental and Computational Study. *Arab. J. Sci. Eng.* **2020**, *45*, 4773–4783. [CrossRef]
8. Hegazy, M.; Rashwan, S.; Kamel, M.; El Kotb, M. Synthesis, Surface Properties and Inhibition Behavior of Novel Cationic Gemini Surfactant for Corrosion of Carbon Steel Tubes in Acidic Solution. *J. Mol. Liq.* **2015**, *211*, 126–134. [CrossRef]

9. Pareek, S.; Jain, D.; Hussain, S.; Biswas, A.; Shrivastava, R.; Parida, S.K.; Kisan, H.K.; Lgaz, H.; Chung, I.-M.; Behera, D. A New Insight into Corrosion Inhibition Mechanism of Copper in Aerated 3.5 wt.% NaCl Solution by Eco-Friendly Imidazopyrimidine Dye: Experimental and Theoretical Approach. *Chem. Eng. J.* **2019**, *358*, 725–742. [CrossRef]
10. Solmaz, R. Investigation of the Inhibition Effect of 5-((E)-4-Phenylbuta-1, 3-Dienylideneamino)-1, 3, 4-Thiadiazole-2-Thiol Schiff Base on Mild Steel Corrosion in Hydrochloric Acid. *Corros. Sci.* **2010**, *52*, 3321–3330. [CrossRef]
11. Xu, B.; Ji, Y.; Zhang, X.; Jin, X.; Yang, W.; Chen, Y. Experimental and Theoretical Studies on the Corrosion Inhibition Performance of 4-Amino-N, N-Di-(2-Pyridylmethyl)-Aniline on Mild Steel in Hydrochloric Acid. *RSC Adv.* **2015**, *5*, 56049–56059. [CrossRef]
12. Chebabe, D.; Abbout, S.; Damej, M.; Oubair, A.; Lakbaibi, Z.; Dermaj, A.; Benassaoui, H.; Doubi, M.; Hajjaji, N. Electrochemical and Theoretical Study of Corrosion Inhibition on Carbon Steel in 1M HCl Medium by 1, 10-Bis (4-Amino-3-Methyl-1, 2, 4-Triazole-5-Thioyl) Decane. *J. Fail. Anal. Prev.* **2020**, *20*, 1673–1683. [CrossRef]
13. Damej, M.; Benassaoui, H.; Chebabe, D.; Benmessaoud, M.; Erramli, H.; Dermaj, A.; Hajjaji, N.; Srhiri, A. Inhibition Effect of 1, 2, 4-Triazole-5-Thione Derivative on the Corrosion of Brass in 3% NaCl Solution. *J. Mater. Environ. Sci.* **2016**, *7*, 738–745.
14. El-Hajjaji, F.; Merimi, I.; Ouasif, L.; Ghoul, M.E.; Achour, R.; Hammouti, B.; Belghiti, M.; Chauhan, D.; Quraishi, M. 1-Octyl-2-(Octylthio)-1H-Benzimidazole as a New and Effective Corrosion Inhibitor for Carbon Steel in 1 M HCl. *Port. Electrochim. Acta* **2019**, *37*, 131–145. [CrossRef]
15. Ma, Q.; Qi, S.; He, X.; Tang, Y.; Lu, G. 1,2,3-Triazole Derivatives as Corrosion Inhibitors for Mild Steel in Acidic Medium: Experimental and Computational Chemistry Studies. *Corros. Sci.* **2017**, *129*, 91–101. [CrossRef]
16. Revie, R.W. *Corrosion and Corrosion Control: An Introduction to Corrosion Science and Engineering*; John Wiley & Sons: Hoboken, NJ, USA, 2008.
17. Kushwaha, A.K.; Sahoo, M.R.; Ray, M.; Das, D.; Nayak, S.; Maity, A.; Sarkar, K.; Bhagat, A.N.; Pal, A.R.; Rout, T.K.; et al. Functional Pyromellitic Diimide as a Corrosion Inhibitor for Galvanized Steel: An Atomic-Scale Engineering. *ACS Omega* **2022**, *7*, 27116–27125. [CrossRef]
18. Kokalj, A.; Lozinšek, M.; Kapun, B.; Taheri, P.; Neupane, S.; Losada-Pérez, P.; Xie, C.; Stavber, S.; Crespo, D.; Renner, F.U.; et al. Simplistic Correlations between Molecular Electronic Properties and Inhibition Efficiencies: Do They Really Exist? *Corros. Sci.* **2021**, *179*, 108856. [CrossRef]
19. Anantharaj, R.; Banerjee, T. Fast Solvent Screening for the Simultaneous Hydrodesulfurization and Hydrodenitrification of Diesel Oil Using Ionic Liquids. *J. Chem. Eng. Data* **2011**, *56*, 2770–2785. [CrossRef]
20. Yang, X.; Fu, S.; Wang, Q.; Sun, Q.; Zhang, J.; Peng, Y.; Liang, Z.; Li, J. Protective Behaviour of Naphthylamine Derivatives for Steel Reinforcement in the Simulated Concrete Pore Solutions: Detailed Experimental and Computational Explorations. *J. Mol. Struct.* **2022**, *1270*, 133898. [CrossRef]
21. Wang, Q.; Fu, S.; Yang, X.; Sun, Q.; Zhang, J.; Peng, Y.; Zhang, R.; Liang, Z.; Li, J. An Imide-Based Organic Polymer as an Inhibitor for HRB400 Steel in Simulated Concrete Pore Solution: Experimental and Theoretical Calculations. *J. Mol. Struct.* **2022**, *1265*, 133426. [CrossRef]
22. Wang, Q.; Lei, L.; Wang, L.; Cao, Y.; Wen, Y.; Lu, Z.; Shang, W. Study of Functional Perylene Diimides for Corrosion Protection on Aluminum Alloy Surfaces. *J. Taiwan Inst. Chem. Eng.* **2023**, *147*, 104933. [CrossRef]
23. Kohl, M.; Alafid, F.; Bouška, M.; Krejčová, A.; Raycha, Y.; Kalendová, A.; Hrdina, R.; Burgert, L. New Corrosion Inhibitors Based on Perylene Units in Epoxy Ester Resin Coatings. *Coatings* **2022**, *12*, 923. [CrossRef]
24. Yao, J.; Qiu, B.; Zhang, Z.-G.; Xue, L.; Wang, R.; Zhang, C.; Chen, S.; Zhou, Q.; Sun, C.; Yang, C.; et al. Cathode Engineering with Perylene-Diimide Interlayer Enabling over 17% Efficiency Single-Junction Organic Solar Cells. *Nat. Commun.* **2020**, *11*, 2726. [CrossRef] [PubMed]
25. Frisch, M.J.; Trucks, G.W.; Schlegel, H.B.; Scuseria, G.E.; Robb, M.A.; Cheeseman, J.R.; Scalmani, G.; Barone, V.; Petersson, G.A.; Nakatsuji, H. *Gaussian 16, Revision C.01*; Gaussian, Inc.: Wallingford, CT, USA, 2016.
26. Zeng, X.Q.; Jiang, Z.N.; Duan, J.M.; Li, Y.R.; Peng, S.Y.; Dong, C.F.; Zhang, G.A. Developing a Novel Amino Acid Derivative as High-Efficient Green Corrosion Inhibitor for Mild Steel in Acidic Solution: Experiments and First-Principles Calculations. *Ind. Crops Prod.* **2024**, *210*, 118032. [CrossRef]
27. Lu, T.; Chen, F. Multiwfn: A Multifunctional Wavefunction Analyzer. *J. Comput. Chem.* **2012**, *33*, 580–592. [CrossRef]
28. Humphrey, W.; Dalke, A.; Schulten, K. VMD: Visual Molecular Dynamics. *J. Mol. Graph.* **1996**, *14*, 33–38. [CrossRef]
29. Zhu, J.; Zhou, G.; Niu, F.; Shi, Y.; Du, Z.; Lu, G.; Liu, Z. Understanding the Inhibition Performance of Novel Dibenzimidazole Derivatives on Fe (110) Surface: DFT and MD Simulation Insights. *J. Mater. Res. Technol.* **2022**, *17*, 211–222. [CrossRef]
30. Zheng, T.; Liu, J.; Wang, M.; Liu, Q.; Wang, J.; Chong, Y.; Jia, G. Synergistic Corrosion Inhibition Effects of Quaternary Ammonium Salt Cationic Surfactants and Thiourea on Q235 Steel in Sulfuric Acid: Experimental and Theoretical Research. *Corros. Sci.* **2022**, *199*, 110199. [CrossRef]
31. Salarvand, Z.; Amirnasr, M.; Talebian, M.; Raeissi, K.; Meghdadi, S. Enhanced Corrosion Resistance of Mild Steel in 1M HCl Solution by Trace Amount of 2-Phenyl-Benzothiazole Derivatives: Experimental, Quantum Chemical Calculations and Molecular Dynamics (MD) Simulation Studies. *Corros. Sci.* **2017**, *114*, 133–145. [CrossRef]

32. Alamry, K.A.; Aslam, R.; Khan, A.; Hussein, M.A.; Tashkandi, N.Y. Evaluation of Corrosion Inhibition Performance of Thiazolidine-2,4-Diones and Its Amino Derivative: Gravimetric, Electrochemical, Spectroscopic, and Surface Morphological Studies. *Process Saf. Environ. Prot.* **2022**, *159*, 178–197. [CrossRef]
33. Fu, S.; Yang, X.; Peng, Y.; Wang, Q.; Sun, Q.; Zhang, J.; Wang, X.; Liang, Z.; Li, J. Corrosion Behaviors of Tetrasodium Iminodisuccinate (IDS) as an Environmentally Friendly Inhibitor: Experimental and Theoretical Studies. *Coatings* **2023**, *13*, 613. [CrossRef]
34. Li, M.; Fu, S.; Peng, Y.; Sang, T.; Cui, C.; Ma, H.; Dai, J.; Liang, Z.; Li, J. An Extensive Analysis of Isoindigotin Derivatives as Effective Corrosion Inhibitors for Mild Steel in Acidic Corrosive Environments: An Electrochemical and Theoretical Investigation. *Prog. Org. Coat.* **2025**, *200*, 108960. [CrossRef]
35. Peimani, A.; Nasr-Esfahani, M. Application of Anise Extract for Corrosion Inhibition of Carbon Steel in CO 2 Saturated 3.0% NaCl Solution. *Prot. Met. Phys. Chem. Surf.* **2018**, *54*, 122–134. [CrossRef]
36. El-Hashemy, M.A.; Sallam, A. The Inhibitive Action of Calendula Officinalis Flower Heads Extract for Mild Steel Corrosion in 1 M HCl Solution. *J. Mater. Res. Technol.* **2020**, *9*, 13509–13523. [CrossRef]
37. Farag, A.A.; Ismail, A.S.; Migahed, M. Environmental-Friendly Shrimp Waste Protein Corrosion Inhibitor for Carbon Steel in 1 M HCl Solution. *Egypt. J. Pet.* **2018**, *27*, 1187–1194. [CrossRef]
38. El Bribri, A.; Tabyaoui, M.; Tabyaoui, B.; El Attari, H.; Bentiss, F. The Use of Euphorbia Falcata Extract as Eco-Friendly Corrosion Inhibitor of Carbon Steel in Hydrochloric Acid Solution. *Mater. Chem. Phys.* **2013**, *141*, 240–247. [CrossRef]
39. Fernandes, C.M.; Alvarez, L.X.; dos Santos, N.E.; Maldonado Barrios, A.C.; Ponzio, E.A. Green Synthesis of 1-Benzyl-4-Phenyl-1H-1,2,3-Triazole, Its Application as Corrosion Inhibitor for Mild Steel in Acidic Medium and New Approach of Classical Electrochemical Analyses. *Corros. Sci.* **2019**, *149*, 185–194. [CrossRef]
40. Boumezzourh, A.; Ouknin, M.; Chibane, E.; Costa, J.; Bouyanzer, A.; Hammouti, B.; Majidi, L. Inhibition of Tinplate Corrosion in 0.5 M H2C2O4 Medium by Mentha Pulegium Essential Oil. *Int. J. Corros. Scale Inhib.* **2020**, *9*, 152–170.
41. Aljourani, J.; Raeissi, K.; Golozar, M. Benzimidazole and Its Derivatives as Corrosion Inhibitors for Mild Steel in 1M HCl Solution. *Corros. Sci.* **2009**, *51*, 1836–1843. [CrossRef]
42. Sun, Q.; Fu, S.; Peng, Y.; Li, P.; Ma, H.; Fang, Z.; Ma, T.; Zhang, R.; Liang, Z.; Li, J. Isoindigo Derivatives as Some Potential Corrosion Inhibitors for Mild Steel in Hydrochloric Acid Solution: Synthesis, Experimental and Theoretical Studies. *J. Mol. Struct.* **2024**, *1312*, 138480. [CrossRef]
43. Fu, S.; Peng, Y.; Sun, Q.; Wang, Q.; Li, P.; Ma, H.; Fang, Z.; Ma, T.; Du, S.; Liang, Z.; et al. A Comprehensive Study of Highly Soluble Cationic Polyfluorene as a Polymer Anticorrosive Coating: Anticorrosion Mechanisms and Performance Evaluation. *Prog. Org. Coat.* **2024**, *191*, 108455. [CrossRef]
44. Solomon, M.M.; Umoren, S.A.; Abai, E.J. Poly(Methacrylic Acid)/Silver Nanoparticles Composites: In-Situ Preparation, Characterization and Anticorrosion Property for Mild Steel in H2SO4 Solution. *J. Mol. Liq.* **2015**, *212*, 340–351. [CrossRef]
45. El Aoufir, Y.; Lgaz, H.; Bourazmi, H.; Kerroum, Y.; Ramli, Y.; Guenbour, A.; Salghi, R.; El-Hajjaji, F.; Hammouti, B.; Oudda, H. Quinoxaline Derivatives as Corrosion Inhibitors of Carbon Steel in Hydrochloridric Acid Media: Electrochemical, DFT and Monte Carlo Simulations Studies. *J. Mater. Environ. Sci.* **2016**, *7*, 4330–4347.
46. Damej, M.; Kaya, S.; Ibrahimi, B.E.; Lee, H.; Molhi, A.; Serdaroğlu, G.; Benmessaoud, M.; Ali, I.; Hajjaji, S.E.; Lgaz, H. The Corrosion Inhibition and Adsorption Behavior of Mercaptobenzimidazole and Bis-Mercaptobenzimidazole on Carbon Steel in 1.0 M HCl: Experimental and Computational Insights. *Surf. Interfaces* **2021**, *24*, 101095. [CrossRef]
47. Wang, Q.; Peng, Y.; Fu, S.; Yang, X.; Sun, Q.; Wang, X.; Zhang, J.; Liang, Z.; Li, J. Experimental and Theoretical Investigations of 1,1′-Dibenzyl-[4,4′-Bipyridine]−1,1′-Diium Chloride as Effective Corrosion Inhibitor for Q235 Steel in 1 M HCl. *Mater. Today Commun.* **2023**, *35*, 106169. [CrossRef]
48. Ould Abdelwedoud, B.; Damej, M.; Tassaoui, K.; Berisha, A.; Tachallait, H.; Bougrin, K.; Mehmeti, V.; Benmessaoud, M. Inhibition Effect of N-Propargyl Saccharin as Corrosion Inhibitor of C38 Steel in 1 M HCl, Experimental and Theoretical Study. *J. Mol. Liq.* **2022**, *354*, 118784. [CrossRef]
49. Han, P.; He, Y.; Chen, C.; Yu, H.; Liu, F.; Yang, H.; Ma, Y.; Zheng, Y. Study on Synergistic Mechanism of Inhibitor Mixture Based on Electron Transfer Behavior. *Sci. Rep.* **2016**, *6*, 33252. [CrossRef]
50. Xu, Y.; Zhang, S.; Li, W.; Guo, L.; Xu, S.; Feng, L.; Madkour, L.H. Experimental and Theoretical Investigations of Some Pyrazolo-Pyrimidine Derivatives as Corrosion Inhibitors on Copper in Sulfuric Acid Solution. *Appl. Surf. Sci.* **2018**, *459*, 612–620. [CrossRef]
51. Hsissou, R. Review on Epoxy Polymers and Its Composites as a Potential Anticorrosive Coatings for Carbon Steel in 3.5% NaCl Solution: Computational Approaches. *J. Mol. Liq.* **2021**, *336*, 116307. [CrossRef]
52. Guo, L.; Safi, Z.S.; Kaya, S.; Shi, W.; Tüzün, B.; Altunay, N.; Kaya, C. Anticorrosive Effects of Some Thiophene Derivatives against the Corrosion of Iron: A Computational Study. *Front. Chem.* **2018**, *6*, 155. [CrossRef]

53. Lgaz, H.; Salghi, R.; Masroor, S.; Kim, S.-H.; Kwon, C.; Kim, S.Y.; Yang, Y.-J.; Chung, I.-M. Assessing Corrosion Inhibition Characteristics of Hydrazone Derivatives on Mild Steel in HCl: Insights from Electronic-Scale DFT and Atomic-Scale Molecular Dynamics. *J. Mol. Liq.* **2020**, *308*, 112998. [CrossRef]
54. Boutouil, A.; Laamari, M.R.; Elazhary, I.; Bahsis, L.; Anane, H.; Stiriba, S.-E. Towards a Deeper Understanding of the Inhibition Mechanism of a New 1,2,3-Triazole Derivative for Mild Steel Corrosion in the Hydrochloric Acid Solution Using Coupled Experimental and Theoretical Methods. *Mater. Chem. Phys.* **2020**, *241*, 122420. [CrossRef]

Disclaimer/Publisher's Note: The statements, opinions and data contained in all publications are solely those of the individual author(s) and contributor(s) and not of MDPI and/or the editor(s). MDPI and/or the editor(s) disclaim responsibility for any injury to people or property resulting from any ideas, methods, instructions or products referred to in the content.